LITHOS 544–545 (2026) 108777

Contents lists available at ScienceDirect

LITHOS

journal homepage: www.elsevier.com/locate/lithos

Halogen recycling initiated by sediment subduction: Insights from Mediterranean alkaline rocks☆

Qingxun Luo [a], Chunfei Chen [a,*], Martina Casalini [b,c], Dejan Prelević [d], Sandro Conticelli [b,c], Michael W. Förster [e], Stephen F. Foley [e], Xu Xiao [a], Tao He [a], Zhaochu Hu [a], Yongsheng Liu [a,f]

[a] State Key Laboratory of Geological Processes and Mineral Resources, School of Earth and Planetary Sciences, China University of Geosciences, Wuhan 430074, China
[b] Dipartimento di Scienze della Terra, Università degli Studi di Firenze, Via Giorgio La Pira, 4, I-50121 Firenze, Italy
[c] Consiglio Nazionale delle Ricerche – Istituto di Geologia Ambientale e Geoingegneria, Area della Ricerca Roma 1, Strada Provinciale 35d, 9-00010 Montelibretti, Italy
[d] Faculty of Mining & Geology, University of Belgrade, Djušina 7, 11 000 Belgrade, Serbia
[e] Research School of Earth Sciences, Australian National University, Canberra, Australian Capital Territory, Australia
[f] Yangtze University, Jingzhou 434000, China

ARTICLE INFO

Keywords:
Halogens
Alkaline rocks
Sediment
Subduction zones

ABSTRACT

Slab subduction is the only efficient mechanism for recycling halogens from the Earth's surface into the interior, thereby regulating long-term ocean salinity and sustaining the Earth's habitability. Dehydration and melting are the two principal pathways by which subducted slabs transfer surface-derived halogens into the mantle. Previous constraints on halogen behavior in subduction zones have been broadly established based on fluid-dominated arc lavas and metamorphic rocks. However, the compositions and behavior of halogens during slab melting, and their role in subduction-zone halogen cycling, remain poorly constrained. Here we present bulk-rock halogen (F and Cl), C, and S data for two Mediterranean alkaline suites formed in a subduction-related setting–leucite-bearing rocks and orogenic lamproites–interpreted to be derived from the lithospheric mantle metasomatized predominantly by carbonate-rich and siliciclastic sediment melts, respectively. Both leucite-bearing rocks and high-Mg# (>75) lamproites exhibit higher F (1850–3210 and 660–4180 ppm) than N-MORB. In contrast, a subset of lamproites preserve near-primary Cl content (mean ~ 632 ppm), while all leucite-bearing rocks and some of the lamproites show significant Cl depletion due to volcanic degassing. Melting models show that the mantle sources of these alkaline rocks were strongly enriched in halogens (~800 ppm F and ~ 50 ppm Cl), with concentrations equivalent to ~50 times those of the depleted mantle. This suggests that substantial surface F and Cl can be transported into the mantle wedge through sediment subduction. The mantle sources of these alkaline rocks are characterized by high F/Cl (~4.7) and by F/Nd (~20.7) and Cl/Nb (~16.8) ratios that fall within the ranges of dehydrated subducted sediments and primary N-MORB. This contrasts sharply with dehydration-dominated arc lavas, which exhibit low F/Cl (~0.58), elevated F/Nd (~34.1), and extremely high Cl/Nb (~1315). These results indicate that sediment-melt metasomatism enriches F and Cl in the mantle without significantly modifying F/Nd or Cl/Nb, whereas slab-fluid metasomatism preferentially enriches Cl and strongly increases Cl/Nb of the mantle. Our results therefore demonstrate that combined F/Cl, F/Nd, and Cl/Nb systematics provide an effective means of distinguishing the relative contributions of melting and dehydration to halogen recycling in subduction zones.

1. Introduction

Maintaining Earth's habitability requires a persisting balance between deep halogen outgassing through volcanism and surface halogen return to the deep mantle via subduction (Chen et al., 2023). Volcanism at mid-ocean ridges, ocean islands, and island arcs represents the main route of halogen outflux from the mantle. In contrast, subduction acts as the only efficient pathway for halogen influx back into the mantle, thereby regulating ocean salinity throughout geological history and contributing to Earth's habitability (Hanyu et al., 2019; Wang and Xu,

☆ This article is part of a Special issue entitled: 'Steve Foley Special Issue' published in LITHOS.

* Corresponding author.
E-mail address: chfchen2016@hotmail.com (C. Chen).

https://doi.org/10.1016/j.lithos.2026.108777
Received 27 April 2026; Received in revised form 7 September 2026; Accepted 11 September 2026
Available online 25 September 2026
0024-4937/© 2026 Elsevier B.V. All rights are reserved, including those for text and data mining, AI training, and similar technologies.

2024).

Crustal materials subducted into the mantle may undergo slab dehydration, melting, and diapirism, driving arc volcanism that returns part of their halogen budget to the surface, while the residual slab continues to transport remaining halogens into the deep mantle (Chen et al., 2021; Chen et al., 2023; Kendrick et al., 2014; Straub and Layne, 2003). It is therefore critical to constrain halogen partitioning and fractionation associated with dehydration, melting, and diapirism during slab subduction. Halogen behavior during slab dehydration has been widely investigated (e.g., John et al., 2011; Kendrick et al., 2020; Maunder et al., 2024). Overall, aqueous fluids released during dehydration of the oceanic slab are characterized by low F/Cl. In particular, sedimentary pore fluids released during shallow compaction are characterized by elevated Br/Cl and I/Cl (Muramatsu et al., 2001; Muramatsu et al., 2007), whereas dehydration of altered oceanic crust (AOC) and serpentinized lithosphere yields MORB-like Br/Cl and more variable I/Cl (Kendrick et al., 2014; Kendrick et al., 2020). Diapirism has also been proposed as a potential pathway for transporting crustal materials, including halogens, from the subducting slab through the overlying mantle wedge and ultimately to the surface via arc volcanism (Behn et al., 2011; Marschall and Schumacher, 2012). However, a recent study on Mariana arc magmatism indicated that the contribution of direct melting of mélange diapirism to arc-magmatic halogen budgets is likely minor (Maunder et al., 2024). Slab melting is most likely restricted to hot slab settings, particularly during subduction of young oceanic lithosphere (< 25 Ma) and under geodynamic conditions that enhance heat input (Defant and Drummond, 1990; Gutscher et al., 2000). Experiments on slab melting indicate that sediments melt before igneous crust and that the resulting slab-derived melts can efficiently transport key subduction zone components, including halogens (Gerya and Yuen, 2003; Klemme et al., 2002; Li et al., 2022; Mann and Schmidt, 2015). Nevertheless, halogen composition and partitioning during slab melting, how slab melts contribute to halogen cycling in arc magmatism, and how to distinguish slab-melt halogen signatures from those of slab fluids remain poorly constrained.

In this study, we investigate F and Cl contents and their ratios to similarly incompatible elements (F/Nd and Cl/Nb) in Mediterranean leucite-bearing rocks and lamproites formed in a subduction-related setting. These rocks record metasomatism by carbonate-rich and siliciclastic sediment-derived components, respectively (e.g., Boari et al., 2009; Conticelli et al., 2015; Prelević et al., 2012). We have also compiled the bulk-rock halogen and trace element datasets of global slab fluid-induced arc-related lavas (forearc, arc, and backarc), mid-ocean ridge basalts (MORBs) and ocean island basalts (OIBs) for comparison (Supplementary Table 1). Our aims are to evaluate the behavior of halogens during slab melting associated with subducted sediments to better constrain the halogen partitioning and fractionation during slab dehydration versus melting and during slab-mantle interaction. This enables us to assess how these processes contribute to halogen recycling signatures recorded by global MORBs and OIBs.

2. Geological setting and sample description

The present-day Mediterranean domain comprises a system of fold-and-thrust belts, flanked by foreland basins and punctuated by back-arc basins, reflecting protracted convergence between the Eurasian and African–Arabian plates and the stepwise closure of the Paleotethys and the Neotethys oceans (Cavazza et al., 2004; Cavazza and Wezel, 2003). Across the wider Alpine–Tethyan belt, alternating phases of oceanic subduction, continental collision, slab rollback and tearing, and subsequent extension produced a linked chain of orogens and hinterland basins, including the Alps–Apennines, the Dinarides–Vardar zone, and the Anatolian orogenic system (Cavazza et al., 2004; Cavazza and Wezel, 2003; El-Sharkawy et al., 2020; Schmid et al., 2020).

In the western Mediterranean, subduction initiated during Late Cretaceous convergence culminated in early Eocene continental collision and construction of the Alpine orogen. Subduction was subsequently reorganized into a west-dipping system along the Corsica–Sardinia–Adria margin, and eastward rollback of the Adriatic–Ionian slab drove Apennine orogenesis and the opening of the Ligur-o–Provençal and Tyrrhenian back-arc basins, with active subduction today largely confined to the Calabrian arc (Avanzinelli et al., 2009; Faccenna et al., 2001; Peccerillo and Frezzotti, 2015). Farther east, the Dinaride–Vardar segment preserves a record of Mesozoic subduction of Vardar oceanic lithosphere beneath southern Eurasia, widespread ophiolite emplacement, and growth of a double-vergent Dinaride orogen, followed by Late Cretaceous collision involving Adria-affinity continental fragments and the European margin (Robertson et al., 2009; Slovenec and Pamić, 2002; Ustaszewski et al., 2010). At the eastern termination of the belt, southwestern Anatolia evolved after final Neotethyan closure from crustal thickening to Neogene back-arc-like extension driven by rollback and tearing of the African slab beneath the Hellenic–Cyprus arc. This promoted exhumation of the Menderes core complex, E–W graben formation, and lithospheric thinning (e.g., Erman et al., 2022; Prelević et al., 2005).

The leucite-bearing rocks studied here are silica-undersaturated volcanic rocks from the Colli Albani Volcanic District within the Roman Magmatic Province in Italy (Boari et al., 2009). They are largely aphyric to sub-aphyric and their phenocrysts are dominantly leucite and clinopyroxene, with olivine occurring only as a minor and sporadic phase. Accessory minerals in the groundmass are scarce and include apatite, calcite, Ti-magnetite, and nepheline. They display strong enrichment in large-ion lithophile elements (LILE) and Sr-Nd-Pb isotopic signatures characterized by variably radiogenic Sr and Pb coupled with unradiogenic Nd, collectively indicating contributions from recycled carbonate-rich sediments introduced into their mantle source (Avanzinelli et al., 2009; Boari et al., 2009; Conticelli et al., 2015). The lamproite samples are from southwestern Anatolia (Turkey) and Serbia; they show similarly extreme LILE enrichment, pronounced negative Nb–Ti anomalies, and radiogenic Sr with unradiogenic Nd. These features are commonly interpreted to reflect partial melting of strongly metasomatized lithospheric mantle that had been refertilized by slab-derived siliciclastic sediment components (e.g., Prelević et al., 2005; Prelević et al., 2008).

The detailed petrography, major-, trace- element and isotopic compositions of these alkaline suites have been described previously (e.g., Boari et al., 2009; Conticelli et al., 2015; Prelević et al., 2007; Prelević et al., 2012). The samples analyzed in this study are generally fresh and show only limited effects of weathering and post-magmatic alteration (e.g., Boari et al., 2009; Ren et al., 2024). Published petrographic observations indicate that the leucite-bearing rocks preserve fresh primary assemblages of leucite and clinopyroxene, with subordinate olivine and melilite (Boari et al., 2009). Similarly, the lamproites retain primary high-Fo olivine, commonly containing Cr-spinel inclusions, together with fresh phlogopite, clinopyroxene, and variably crystalline igneous groundmass assemblages (Prelević et al., 2012). The detailed major element data are provided in Supplementary Table 1.

3. Methods

3.1. Bulk-rock halogen analysis

Bulk-rock F concentrations were determined at the ALS Chemex Laboratory in Guangzhou, China. Samples were digested by alkaline fusion with potassium hydroxide, and F was quantified using an ion-selective electrode (Metrohm IC930). The detection limit was 20 ppm, and analytical uncertainties were better than 5%. Accuracy was monitored by analyzing reference materials JR-1, NCSDC71302, and NCSDC73029, which yielded F concentrations consistent with published reference values within analytical error (Table 1).

Bulk-rock Cl concentrations were measured at the State Key Laboratory of Geological Processes and Mineral Resources, China University

Table 1
Halogen, carbon, and sulfur concentrations of reference materials measured in this study.

	Standard materials	Recommended value	Measured value
F	JR-1	990 ppm	990 ppm
	NCSDC71302	1120 ppm	1110 ppm
	NCSDC73029	670 ppm	660 ppm
Cl	BCR-2	89–112 ppm[a,b,c,d]	89 ppm
	BHVO-2	81–104 ppm[a,b,c,e]	86 ppm
C	In-house standard (steel)	3.90 wt%	3.91 wt%
S	In-house standard (steel)	0.05 wt%	0.05 wt%

[a] Kobayashi et al. (2021).
[b] Wang et al. (2010)
[c] Sekimoto and Ebihara (2017).
[d] Hanano et al. (2010).
[e] Balcone-Boissard et al. (2009).

of Geosciences, Wuhan. Sample preparation followed the efficient NH_4HF_2 digestion protocol described in He et al. (2019). Briefly, ~100 mg of rock powder was digested with purified NH_4HF_2 at 220 °C for 2 h. During digestion, an alkaline atmosphere generated by NH_3 minimizes potential halogen loss. Aliquots of Te solution (10 μg/L) were added to the supernatant as an internal standard prior to analysis. Chlorine was quantified in the supernatant using a high-sensitivity sector-field ICP-MS (Element XR) at medium-resolution mode. The method detection limit for Cl was 5 μg/g. Analytical accuracy was monitored by repeated analyses of the reference materials BHVO-2 and BCR-2, which yielded Cl concentrations consistent with published reference values within analytical uncertainty (Table 1).

3.2. Bulk-rock carbon and sulfur analysis

Bulk-rock C and S contents were determined at the State Key Laboratory of Geological Processes and Mineral Resources, China University of Geosciences, Wuhan, using a high-frequency infrared C–S analyzer. The instrument was calibrated prior to measurements using an in-house steel reference standard. Analytical accuracy and session stability were assessed by repeated analyses of the in-house steel standard, which produced C and S values consistent with published reference concentrations within analytical uncertainty (Table 1). Each sample was measured in triplicate, and the in-house steel standard was reanalyzed after every three samples to track instrumental drift during the analytical run (Wang et al., 2025).

Table 2
Halogen, carbon, and sulfur contents of alkaline rocks from the Mediterranean region.

Sample	Location	F[a]	Cl[a]	1SD	C[a]	1SD	S[a]	1SD
		ppm	ppm		ppm		ppm	
Leucite-bearing rocks								
VLS 02	Colli Albani, Italy	2290	28.4	1.2	1856	165	39.3	11.2
R-VLS 02[b]	Colli Albani, Italy		38.1	2.9				
VLS 05	Colli Albani, Italy	3210	224.3	4.8	4232	397	106.0	15.1
VLS 11	Colli Albani, Italy	1950	59.2	0.8	6766	71	316.1	10.7
VLS 12	Colli Albani, Italy	2280	19	0.3	2172	18	62.9	2.5
VLS 15	Colli Albani, Italy	2800	60.4	1.8	860	40	15.9	10.3
VLS 20	Colli Albani, Italy	2620			2106	11	29.9	6.9
VLS 25	Colli Albani, Italy	2280	49.3	2.8	1672	59	21.0	3.0
VLS 26	Colli Albani, Italy	2120	22.7	2.5	279	41	6.1	7.4
VLS 35	Colli Albani, Italy	1850	34.7	2.1	561	20	14.4	10.0
VLS 38	Colli Albani, Italy	2210	46.1	4.8	1773	18	45.8	9.7
VLS 43	Colli Albani, Italy	2030	24.4	2.4	528	7	3.7	3.9
VLS 50	Colli Albani, Italy	2420			383	26	16.0	4.9
CA 07juve	Colli Albani, Italy	2120			5394	103	146.3	12.5
CA 12	Colli Albani, Italy	2480			239	11	5.2	4.8
CA 13	Colli Albani, Italy	1900			297	18	25.4	1.8
CA 21	Colli Albani, Italy	2020			197	16	6.4	3.0
Orogenic lamproites								
03 V16	Murcia–Almería, Spain	2700	763.6	4.4				
03 J10	Murcia–Almería, Spain	3160	817.6	10.2	1874	50	505.6	6.4
03FC01	Murcia–Almería, Spain	3150	360.7	6.3	2566	26	123	15.6
04CR02	Vardar Zone, North Macedonia		481.1	3.1				
04CR01	Vardar Zone, North Macedonia		67.9	0.8	542		10.3	
04SL01	Vardar Zone, North Macedonia		171.1	2.3				
03KK04	Vardar Zone, North Macedonia		213.4	17.5	623	15	14.6	17.7
05RR02	Western Alps, Italy	3120	465	3.3	995	29	27	14.9
05GV02	Western Alps, Italy	1570	168.9	1.8				
05KD01	Western Anatolia, Turkey	1590	153.3	1.8				
05KD03	Western Anatolia, Turkey		179.2	1.4	497	18	0.1	0.1
05KD012	Western Anatolia, Turkey	4180	151.2	1.5	242	20	0.5	0.7
05KD14	Western Anatolia, Turkey	660	1244.4	11.4				
06KD21	Western Anatolia, Turkey	4130	155.2	2.3	823	96	20.9	0.5
05IS01	Western Anatolia, Turkey	3840	100.7	1.1	2343	44	6	5.8
05BH05	Western Anatolia, Turkey	4050	87.9	4.1	13,118	47	2.1	2.8
BK01/3–1	Vardar Zone, Serbia	2670	38.3	1.9	920	28	6.6	9.7
BK01/3C	Vardar Zone, Serbia	2230	192.1	2.7	447	7	2.8	4.8
BK01/3A-2	Vardar Zone, Serbia	2400	43.8	0.2				
Bo2–2	Vardar Zone, Serbia		163		1308	18	2.2	3.0

[a] Analytical uncertainty for F is less than 5%, whereas those for Cl, C, and S are reported as 1SD.
[b] R-VLS 02 are duplicate analyses of VLS 02 and yielded comparable results.

4. Results

The F, Cl, C, and S contents of the alkaline rocks are presented in Table 2. Both the leucite-bearing rocks and lamproites are enriched in F (1850–3210 ppm and 660–4180 ppm, respectively) relative to that in MORBs (60–1308 ppm) and overlap with those in kimberlites (804–5399 ppm) and OIBs (62–2637 ppm; Fig. 1a). In contrast, their Cl abundances broadly overlap those of MORBs and OIBs (Fig. 1a). The leucite-bearing rocks show relatively restricted and generally lower Cl concentrations (19.0–224.3 ppm; mean = 56.8 ppm), whereas the lamproites display a much wider range (38.3–1244 ppm) and a markedly higher mean Cl concentration (301 ppm) than that of the leucite-bearing rocks (Table 2; Fig. 1a). A similarly broad, but more extreme, range is observed in kimberlites (9–14,000 ppm; Fig. 1a). Compared to MORBs and OIBs, the leucite-bearing rocks and lamproites exhibit higher F/Cl ratios (14.3–119.7 and 0.5–69.7; Fig. 1a). The compiled arc-related lavas from the Marianas and SW Pacific, including forearc, arc and backarc settings, display halogen characteristics distinct from those of the alkaline rocks studied here, with elevated Cl contents relative to N-MORB (mean ~ 898 ppm) but similar F contents (mean ~ 254 ppm), resulting in low F/Cl ratios overall (average 0.58; Fig. 1a).

Carbon and sulfur concentrations in the leucite-bearing rocks are highly variable (196.8–6766 ppm C; 3.7–316.1 ppm S) and show a strong positive correlation (R^2 = 0.80; Fig. 1b). Lamproites contain 241.9–13,118 ppm C and 0.1–505.6 ppm S.

5. Discussions

5.1. Effects of secondary alteration and crustal contamination

Secondary processes, including post-magmatic hydrothermal alteration (e.g., serpentinization and chloritization) and surface weathering, could substantially modify bulk-rock halogen contents (Frezzotti and Ferrando, 2018; Teiber et al., 2014). Serpentinization typically elevates bulk-rock halogen contents, particularly Cl (Kendrick, 2024; Pagé and Hattori, 2019), which would result in a decrease in bulk-rock F/Cl. In contrast, chloritization may mobilize substantial amounts of F and Cl and potentially lead to depletion of these elements in the bulk rock (Teiber et al., 2014; Zheng et al., 2023). Our alkaline rocks are exceptionally fresh and no secondary alteration minerals (e.g., serpentine or chlorite) were observed. They are characterized by high F contents and high F/Cl ratios (Fig. 1a), which are inconsistent with Cl enrichment or F loss associated with serpentinization and chloritization. Moreover, F, Cl, and F/Cl show no systematic relationships with fluid-mobile elements (e.g., Rb, Ba, and Pb) which are commonly enriched during hydrothermal alteration, arguing against significant hydrothermal overprinting. Surface weathering commonly causes depletion of mobile elements, including Cl, Ca, and Mg (Néron et al., 2018; Sha and Chappell, 1999; Teiber et al., 2014), whereas the alkaline rocks studied here generally retain high CaO and MgO contents and show no systematic relationships between these oxides and halogens. Moreover, loss on ignition (LOI) values of the alkaline rocks are low (mostly <2 wt%), and their halogen contents show no correlation with LOI (Fig. 2). Only a few samples have higher LOI (2.99 to 10.93 wt%), yet their halogen contents are indistinguishable from those of the low-LOI samples. The elevated LOI in these few samples is most plausibly attributed to primary igneous components (e.g., amphibole and phlogopite) in the groundmass (Boari et al., 2009; Prelević et al., 2007; Prelević et al., 2012). Overall, secondary alteration exerted a negligible influence on the halogen content of the alkaline rocks.

The upper continental crust is characterized by lower F/Nd and Cl/Nb ratios than MORB (mean ~ 15.8 and ~ 2.5–7.2, respectively; Han et al., 2023). Significant assimilation of upper crustal material is therefore expected to lower whole-rock F/Nd and Cl/Nb below the N-MORB range (Kjarsgaard et al., 2009; Tappe et al., 2013). Previous studies have shown that the alkaline rocks in this study have experienced negligible crustal contamination during magma ascent (Boari et al., 2009; Prelević et al., 2007; Prelević et al., 2012), supported by several lines of evidence: (1) the absence of systematic covariation between $^{87}Sr/^{86}Sr$ or εNd(t) and indices of magmatic differentiation (e.g., SiO_2 and MgO); (2) incompatible trace element abundances far higher than those of the continental crust; and (3) the presence of mafic mineral phases (e.g., high-Fo olivine and clinopyroxene) that are in equilibrium with their host bulk compositions. Furthermore, the alkaline rocks studied here display N-MORB-like or higher F/Nd ratios (Fig. 3a), indicating limited crustal modification of their F contents. Although some alkaline rocks show relatively low Cl/Nb ratios (Fig. 3b), their Cl contents show no systematic relationship with indicators of crustal contamination (e.g., Nb/U). This suggests that crustal contamination made only a limited contribution to the low Cl/Nb values, which were more likely produced by other processes, such as degassing. These observations indicate that crustal contamination did not significantly affect the halogen contents of the studied alkaline rocks.

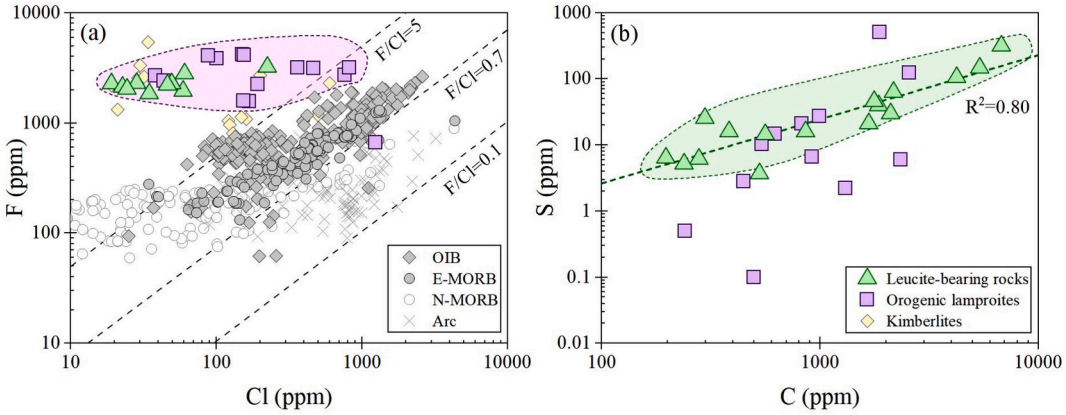

Fig. 1. Log-log plots of F versus Cl (a) and C versus S (b) for the Mediterranean alkaline rocks investigated in this study. Compared to MORBs, OIBs, and arc-related lavas worldwide, the F contents of our alkaline rocks are at a high level (purple field). The leucite-bearing rocks show strong correlations between C and S (R^2 = 0.80; green field). Halogen data of *E*-MORB and N-MORB (Kendrick et al., 2017; Shimizu et al., 2016), OIB (Cabral et al., 2014; Hanyu et al., 2019; Jackson et al., 2015; Kendrick et al., 2017; Kirstein et al., 2023; Sides et al., 2014; Sisson et al., 2009), arc-related lava (Kendrick et al., 2020; Maunder et al., 2024), and kimberlites (Abersteiner et al., 2018; Hoare et al., 2021; Toyama et al., 2021) are shown for comparison. Detailed data are provided in Supplementary Table 1. (For interpretation of the references to colour in this figure legend, the reader is referred to the web version of this article.)

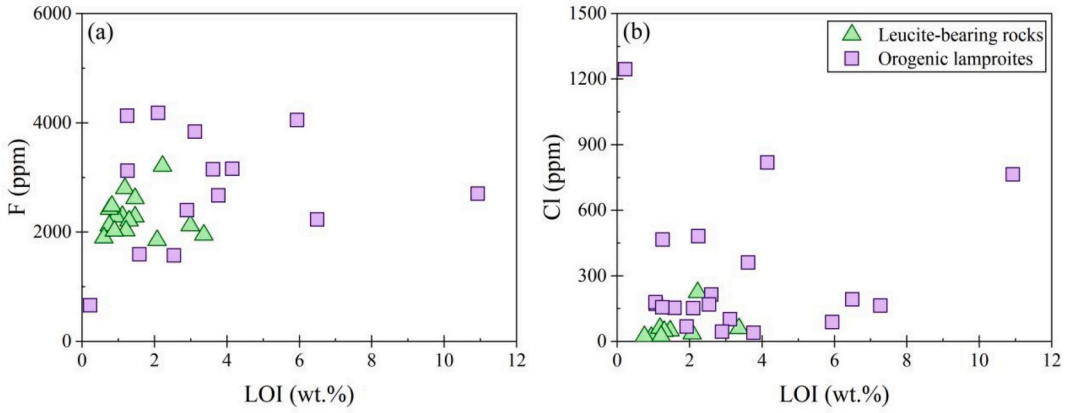

Fig. 2. Plots of F and Cl contents versus Loss on Ignition (LOI) for the Mediterranean alkaline rocks investigated in this study.

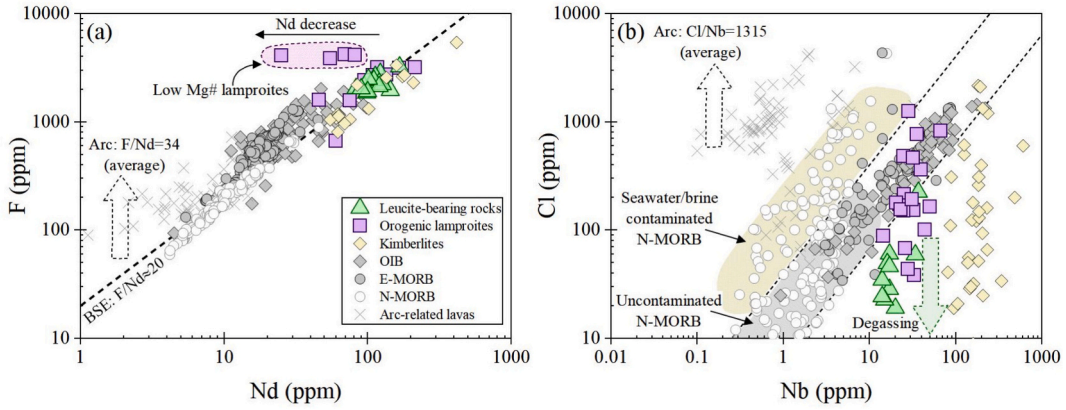

Fig. 3. Log-log plots of F and Cl contents versus similarly incompatible lithophile trace elements (Nd and Nb) for the Mediterranean alkaline rocks investigated in this study. (a) Both the leucite-bearing rocks and the orogenic lamproites exhibit F/Nd ratios consistent with the bulk silicate Earth (BSE) and N-MORB, except for a few low-Mg# lamproites. (b) All leucite-bearing rocks and a subset of the lamproite suite display lower Cl/Nb than primary N-MORB (grey field), suggesting Cl loss through degassing. The F/Nd ratio of BSE is from McDonough and Sun (1995). Data sources for MORB, OIB, and arc lavas are the same as those in Fig. 1.

5.2. *Effects of volcanic degassing*

Fluorine is weakly volatile and is preferentially retained in melts relative to coexisting fluids (Villemant et al., 2008). The alkaline rocks studied here display F/Nd ratios similar to or higher than those of N-MORB (Fig. 3a), indicating that F was not significantly affected by degassing. Chlorine, C, and S are more fluid-mobile and volatile, and therefore partition strongly into magmatic fluids and volcanic gases (Cadoux et al., 2018; Webster et al., 2018).

The leucite-bearing rocks are characterized by relatively lower Cl contents (mean = 56.8 ppm) and Cl/Nb ratios (mean = 2.6) than those of MORB (Fig. 3b), indicating that they may have experienced substantial Cl loss during degassing. In contrast, five of the twenty lamproites are inferred to more closely preserve primary-magmatic Cl signatures, as indicated by their high mean Cl content (754.4 ppm) and Cl/Nb ratios of 12.2–43.7, which overlap those of MORB and OIB (Fig. 3b). The remaining fifteen lamproites have distinctly lower Cl/Nb ratios of 1.2–9.1 (Fig. 3b), consistent with variable Cl loss during degassing. Accordingly, the high-Cl/Nb lamproites may provide a better approximation of the primary-melt Cl characteristics than these low-Cl/Nb lamproites.

During magmatic degassing, C and S are generally lost more readily than Cl (Lesne et al., 2011; Villemant et al., 2008). The leucite-bearing rocks show low C and S contents and a strong positive correlation between C and S ($R^2 = 0.80$; Fig. 1b), indicating that their C and S experienced extensive degassing, which is also consistent with their extremely low Cl contents (Fig. 1a). In contrast, the weaker C–S relationship in the lamproites suggests that degassing of their C and S is less extensive than that in the leucite-bearing rocks. The different degrees of degassing between the two alkaline suites were likely controlled by differences in magma emplacement style. The leucite-bearing magmas erupted explosively and likely experienced extensive degassing (Boari et al., 2009), whereas the lamproitic ones were emplaced predominantly as shallow-level intrusions (Casalini et al., 2022; Prelević et al., 2007) for which higher confining pressures imposed by the overlying crust likely suppressed degassing (Zheng et al., 2023).

5.3. *Effects of mantle melting and magmatic differentiation*

Experimental mineral–melt partitioning studies indicate that both F and Cl are incompatible during peridotite melting under nominally anhydrous conditions, with bulk peridotite–melt partition coefficients of $D_F^{peridotite/melt} = 0.056 \pm 0.002$ and $D_{Cl}^{peridotite/melt} = 0.0019 \pm 0.0004$ (Dalou et al., 2012; Dalou et al., 2014), so the absolute halogen abundances can be significantly modified by magmatic processes including partial melting and magmatic differentiation. Therefore, we use ratios of halogen and trace elements (F/Nd and Cl/Nb) to trace halogen characteristics of the mantle source in these alkaline rocks. Fig. 4 shows the relationships between the magmatic differentiation index Mg# ($100*Mg^{2+}/(Mg^{2+}+Fe^{2+})$ in mol) and F/Nd and Cl/Nb. The leucite-bearing rocks exhibit a relatively narrow Mg# range and show no correlation between F/Nd and Mg# (Fig. 4a), suggesting that their F/Nd

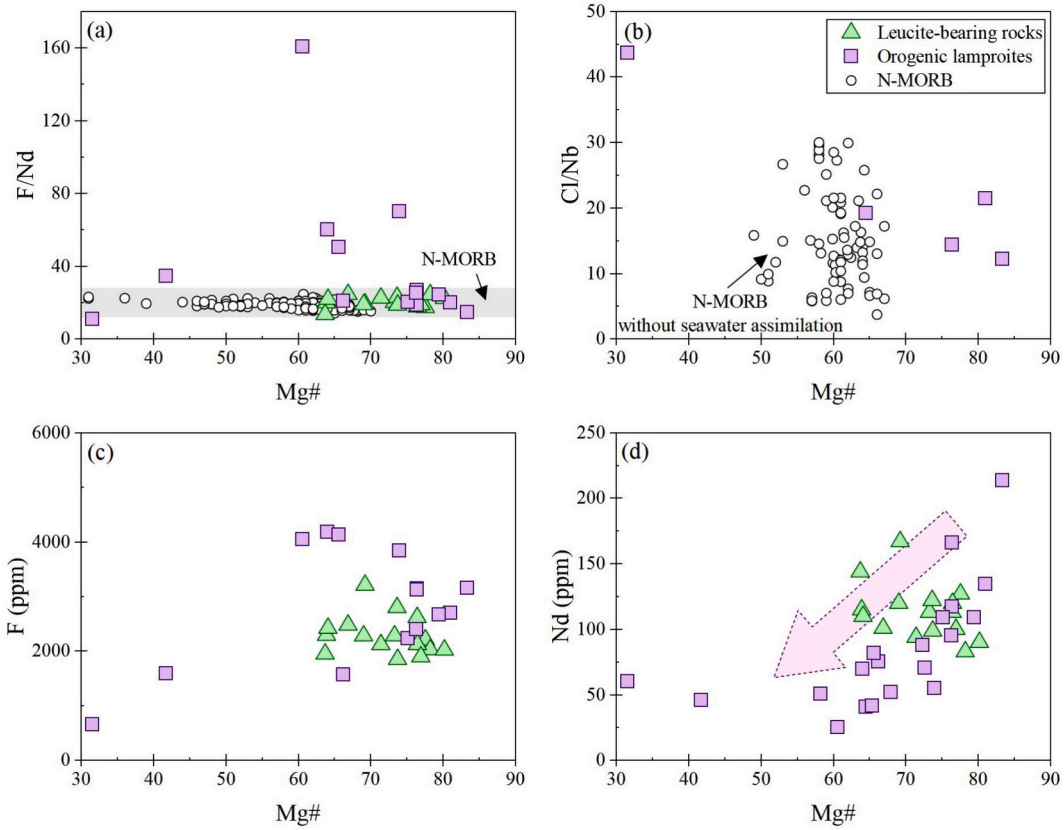

Fig. 4. Plots of Mg# ($100*Mg^{2+}/(Mg^{2+}+Fe^{2+})$ in mol) versus F/Nd, Cl/Nb ratios, F, and Nd contents for the Mediterranean alkaline rocks investigated in this study. F/Nd and Cl/Nb data for N-MORB are also shown for comparison (Kendrick et al., 2017; Shimizu et al., 2016). Only N-MORB samples with no evidence of significant seawater assimilation are included (Cl/Nb < 30; Le Voyer et al., 2015).

ratios (13.5–24.6) predominantly reflect the characteristics of the primary magmas. The high-Mg# (>75) lamproites display relatively limited F/Nd variability (14.8–26.9), whereas low-Mg# lamproites show strongly elevated F/Nd ratios (up to 160.8; Fig. 4a). The anomalously high F/Nd ratios of the low-Mg# lamproites may reflect the preferential removal of Nd from the melt through the crystallization of Nd-bearing mineral phases, as suggested by the strong positive correlation between Nd and Mg#, whereas F shows no systematic variation with Mg# (Fig. 4c, d). We therefore infer that high-Mg# lamproites (>75) provide the best approximation to the F/Nd signature of the primary lamproitic magmas.

The leucite-bearing rocks and most of the lamproites experienced substantial Cl loss during degassing, so their Cl/Nb ratios cannot be used to infer mantle source characteristics. We therefore consider only the lamproites with limited Cl degassing for discussion of the effects of magmatic differentiation on Cl/Nb ratios. The lamproite with the lowest Mg# (31.6), which also has the highest Cl/Nb ratio (43.66), was excluded from this assessment. The remaining lamproites display relatively uniform Cl/Nb ratios of 12.2–21.5 and show no systematic correlation between Cl/Nb and Mg# (Fig. 4b), suggesting that their Cl/Nb was not significantly modified by magmatic differentiation and may approximate the characteristics of the primary lamproitic magmas.

F and Nd, as well as Cl and Nb, are generally regarded as having broadly similar incompatibilities during mantle melting and are therefore not readily fractionated from one another, as evidenced by their strong covariation in global MORB and OIB datasets (Kendrick et al., 2017). However, the alkaline rocks studied here were derived from melting of phlogopite-bearing veins and surrounding peridotite (e.g., Ammannati et al., 2016; Casalini et al., 2022; Conticelli et al., 2015), and the extent to which residual phlogopite modifies melt F/Nd and Cl/Nb remains uncertain. The lamproites studied here show a positive correlation between F and K_2O (Fig. 5a), which may be explained by melting of variable proportions of phlogopite-bearing veins and surrounding peridotite (e.g., Foley, 1989). In comparison, the leucite-bearing rocks display a narrower range of K_2O, suggesting a more uniform contribution from the phlogopite-bearing veins. Although experimental studies suggest that residual phlogopite may lower melt F/Nd because F is compatible in phlogopite whereas Nd remains incompatible (e.g., Flemetakis et al., 2021; Foley and Ezad, 2024), both the primitive lamproites and leucite-bearing rocks exhibit F/Nd ratios comparable to those of N-MORB and show no correlation between F/Nd and K_2O (Fig. 5b), which may be explained by the co-melting of Nd-bearing phases like clinopyroxene and accessory apatite (e.g., Grégoire et al., 2000; O'Reilly and Griffin, 2000). This suggests that F/Nd ratios of the studied alkaline rocks were only weakly affected by residual phlogopite during mantle melting.

Cl and Nb are both highly and similarly incompatible in mantle phlogopite, with partition coefficients generally <0.1 (Flemetakis et al., 2021; Schmidt et al., 1999). During melting of phlogopite-bearing mantle sources, the concentrations of both Cl and Nb in residual phlogopite are expected to remain very low, suggesting that residual phlogopite is unlikely to strongly modify melt Cl/Nb. Furthermore, the least degassed alkaline rocks studied here display Cl/Nb ratios within the N-MORB range (Fig. 3b), suggesting that residual phlogopite had only a limited effect on their Cl/Nb ratios. We therefore infer that the F/Nd and Cl/Nb ratios of the primary alkaline magmas studied here broadly reflect the halogen characteristics of their mantle sources.

5.4. Halogen compositions of sediment-metasomatized mantle sources of Mediterranean alkaline rocks

As discussed above, secondary and magmatic processes did not

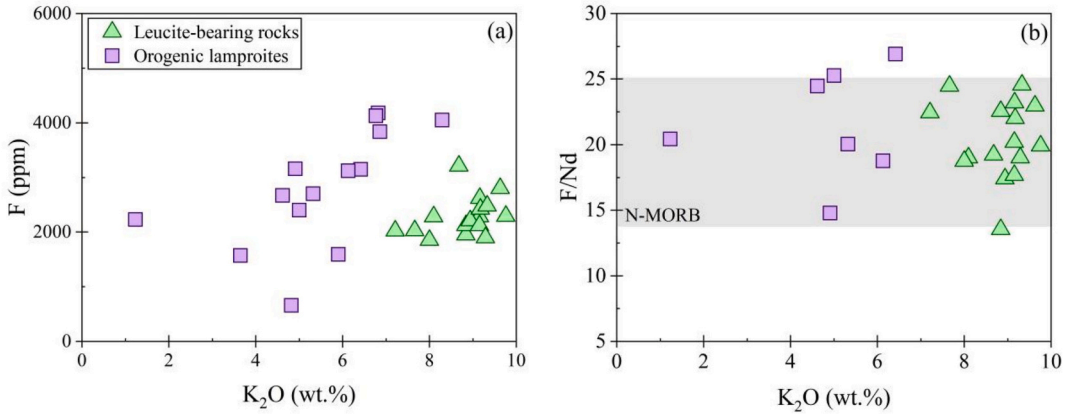

Fig. 5. Plots of F contents and F/Nd ratios versus K_2O contents for the Mediterranean alkaline rocks investigated in this study. (a) The orogenic lamproites show a strong correlation between F and K_2O contents. (b) The F/Nd ratios of the leucite-bearing rocks and primitive lamproites (Mg# > 75) fall within the N-MORB range.

significantly modify the F/Nd and Cl/Nb ratios of the primitive alkaline rocks studied here. Accordingly, the F/Nd ratios of the leucite-bearing rocks and primitive lamproites (Mg# > 75) can be inferred to approximate those in their mantle sources (13.5–24.6 and 14.8–26.9, respectively), and the Cl/Nb of the lamproites without significant degassing can be inferred to approximate that in lamproitic sources (12.2–21.5). Previous studies indicate that the leucite-bearing rocks and lamproites in this study were derived from lithospheric mantle metasomatized predominantly by melts from subducted carbonate-rich and siliciclastic sediment, respectively (e.g., Avanzinelli et al., 2008; Boari et al., 2009; Conticelli et al., 2015; Prelević et al., 2012). The leucite-bearing rocks show stronger carbonate-related signatures, including low SiO_2 (43.7–49.5 wt%), high CaO (9.2–12.3 wt%) and markedly negative Feldspathoid Silica-Saturation Index (FSSI) values (−76.1 to −45.4), whereas primitive lamproites (Mg# > 75) are characterized by higher SiO_2 (46.2–56.2 wt%), lower CaO (3.0–8.4 wt%) and higher FSSI (−6.4–5.8) (Supplementary Table 1; Boari et al., 2009; Casalini et al., 2022). However, the F/Nd ratios of the two alkaline suites overlap substantially and are both comparable to those of N-MORB (Fig. 6a), indicating that the involvement of both carbonate-rich and siliciclastic sediments in their mantle sources did not generate resolvable fractionation of F from Nd, regardless of the presence of carbonate-rich components. In contrast, previous studies suggested that carbonate-rich slab could transport abundant Cl into the deep mantle. Chen et al. (2023) proposed that subduction of carbonate-rich slabs can stabilize chloride and thereby promote Cl recycling into the deep mantle. Hanyu et al. (2019) suggested that carbonated oceanic crust could convey surface-derived Cl into the lower mantle and contribute to the formation of a deep Cl-rich OIB reservoir. In this study, however, these leucite-bearing rocks experienced significant degassing (Fig. 6b), so their Cl contents and Cl/Nb ratios are unlikely to faithfully preserve primary mantle-source signatures. Consequently, the Cl systematics of the leucite-bearing rocks could not be used to constrain the behavior of Cl during carbonate-rich sediment subduction. In the following discussion, we therefore focus only on the Cl contents and Cl/Nb ratios of the lamproites to evaluate Cl behavior during siliciclastic sediment subduction.

To evaluate halogen behavior during melting of sediments, we therefore compare F/Nd and Cl/Nb ratios in the sources of these alkaline rocks with those in subducted sediments. Unlithified pelagic sediments contain ~1000 ppm F and ~ 1 wt% Cl (Kendrick, 2018), together with 27.0 ppm Nd and 8.9 ppm Nb (data from GLOSS; Plank and Langmuir, 1998), corresponding to F/Nd and Cl/Nb ratios of ~37.0 and ~ 1123, respectively. However, sediments would undergo prograde metamorphism and devolatilization during subduction, which can strongly deplete sedimentary halogens. Indeed, eclogite-facies metasediments from the Western Alps have been reported to contain 302.3–779.5 ppm F

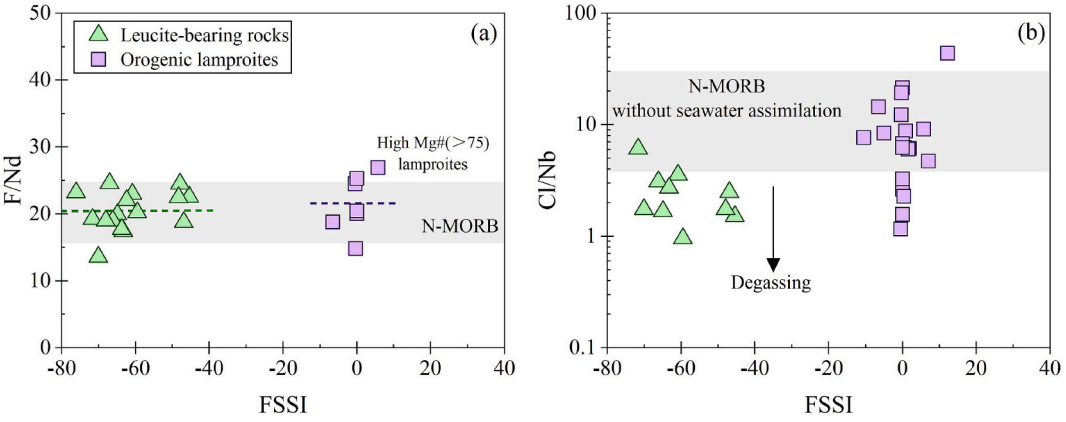

Fig. 6. Plots of feldspathoid silica-saturation index (FSSI) versus (a) F/Nd and (b) Cl/Nb ratios for the Mediterranean alkaline rocks investigated in this study. The FSSI was calculated as normative q − [lc + 2 × (ne + kp)], where q, lc, ne and kp are CIPW normative quartz, leucite, nepheline and kaliophilite, respectively. In this index, normative ne and kp are multiplied by two because each mole of nepheline or kaliophilite requires two moles of quartz to form silica-saturated feldspars (i.e., albite or orthoclase). Negative FSSI values indicate silica-undersaturated compositions, whereas positive values indicate silica-saturated to oversaturated compositions. The grey bands represent the N-MORB reference ranges; in (b), the N-MORB field refers to compositions without seawater assimilation. (a) Colored dashed lines indicate the mean F/Nd ratios of the corresponding rock suites. (b) The downward arrow illustrates the expected effect of degassing, which preferentially lowers Cl/Nb without significantly modifying FSSI.

and 6.2–20 ppm Cl (Hughes et al., 2018), yielding substantially lower F/Nd and Cl/Nb ratios of 11.2–28.9 and 0.7–2.2, respectively. The mantle sources of the alkaline rocks studied here show average F/Nd and Cl/Nb ratios of ~20.7 and ~ 16.8, which are much lower than those of undehydrated sediments and overlap with or are close to the ranges of devolatilized metasediments. These observations indicate that the halogen budget of the mantle sources beneath Mediterranean alkaline rocks was largely influenced by subducted dehydrated sediments.

To quantitatively evaluate the contribution of dehydrated subducted sediments to the halogen budget in the mantle sources of Mediterranean alkaline rocks studied here, we modeled non-modal partial melting (melting degree = 5–30%) of mantle sources assumed at variable initial halogen contents and modal proportions of phlogopite (Fig. 7a and Supplementary Table 2). The initial halogen contents in mantle source were set at 1, 10, and 50 times those of the depleted MORB mantle (DMM; F = 16 ppm, Cl = 1 ppm; Chen, 2025) and the modal proportions of phlogopite were set at 0, 5, and 10% (Fig. 7a). The melting reactions were set as 0.466Cpx + 0.652Opx + 0.049Spl = 0.167Ol + 1.00 melt for phlogopite-free sources (Niu, 1997), and 0.49Phl + 0.56Opx + 0.47Cpx + 0.05Spl = 0.58Ol + 1.00 melt for phlogopite-bearing sources (Condamine and Médard, 2014). The modeling results show that, at DMM-level initial halogen contents, melts derived from phlogopite-free mantle contain 51.1–109.4 ppm F and 3.3–18.3 ppm Cl (Supplementary Table 2), broadly comparable to primitive N-MORB (Fig. 7). In contrast, when the source contains phlogopite and its initial halogen contents are elevated to 50 times those of DMM, the calculated melts contain 2416–4188 ppm F and 167–883 ppm Cl (Supplementary Table 2), overlapping the range of the primitive alkaline rocks with limited

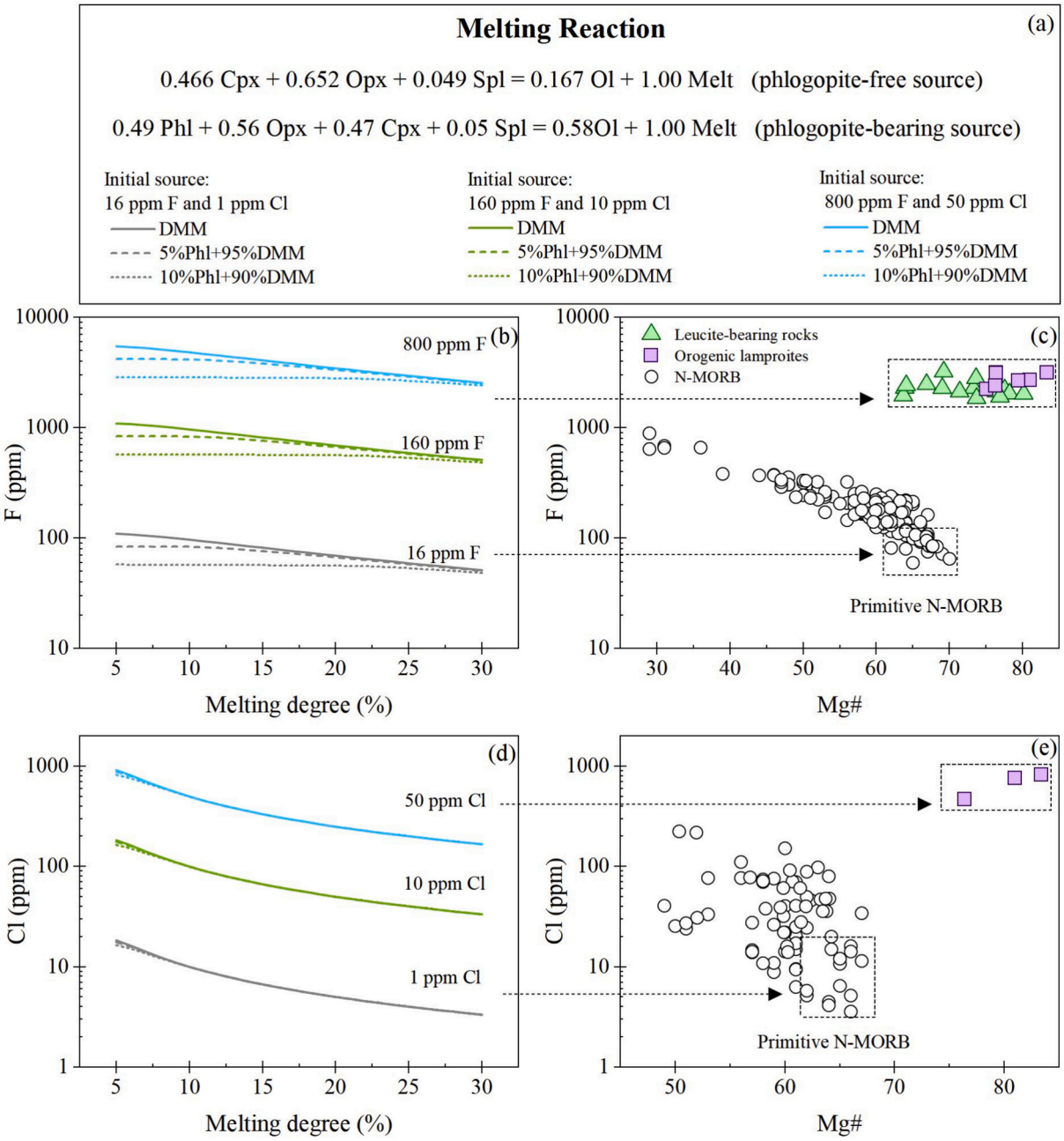

Fig. 7. Modeled F and Cl contents of melt derived from mantle sources at variable initial halogen contents and modal proportions of phlogopite during non-modal melting with increasing degree of melting (5–30%). The melting reactions for phlogopite-free and phlogopite-bearing sources are from Niu (1997) and Condamine and Médard (2014). Details of the partial melting calculation are described in the Supplementary Table 2.

degassing (1850–3210 ppm F and 465–818 ppm Cl; Fig. 7). These results indicate that the mantle sources of the alkaline rocks studied here were substantially enriched in halogens, comparable to ~50 times DMM (800 ppm F and 50 ppm Cl). We therefore conclude that melts derived from dehydrated subducted sediments could extract and transfer substantial amounts of halogens from the subducting slab to the overlying mantle wedge, thereby generating the halogen-enriched mantle sources of the Mediterranean alkaline rocks studied here.

5.5. Key role of melts and fluids on halogen recycling in subduction zones

Melting and dehydration are the two principal mechanisms by which halogens are extracted from the subducting slab. To distinguish halogen behavior during melting versus dehydration of subducted oceanic crust, we compared the F/Cl, F/Nd, and Cl/Nb ratios of Mediterranean alkaline rocks studied here with compiled data of arc-related lavas (forearc, arc, and backarc) from the Marianas and SW Pacific (Kendrick et al., 2020; Maunder et al., 2024). Trace elements of these arc-related lavas indicate the variable involvement of slab-derived aqueous fluids and sediment melts, or both in their mantle sources. In Th/Yb versus Ba/La diagram, two contrasting trends are revealed (Fig. 8). First, the leucite-bearing rocks and lamproites, which are interpreted to originate from mantle domains metasomatized predominantly by melts of sediments, are characterized by low Ba/La and elevated Th/Yb (Fig. 8). Second, arc lavas believed to be derived from mantle sources metasomatized by slab-derived aqueous fluids show high Ba/La and low Th/Yb (blue boxes in Fig. 8). Some arc lavas influenced by both aqueous fluids and sediment melts occupy an intermediate field with low Ba/La and low Th/Yb (yellow boxes in Fig. 8). The halogen systematics of these arc-related lavas can therefore be used to evaluate the roles of slab melting and dehydration in controlling halogen recycling in subduction-zone magmatism (Fig. 9).

Arc magmas dominated by sediment-melt metasomatism, as exemplified by the Mediterranean alkaline rocks studied here, are characterized by F/Cl of ~4.7, and N-MORB-like F/Nd (~20.7) and Cl/Nb (~16.8) (N-MORB: F/Nd ≈ 18.6 and Cl/Nb ≈ 14.9; Figs. 9 and 10). This indicates that sediment-melt metasomatism enriches F and Cl in the mantle source (both ~50 times), while not significantly fractionating F/Nd or Cl/Nb relative to the depleted mantle. In contrast, the collected arc-related lavas influenced predominantly by aqueous slab fluids

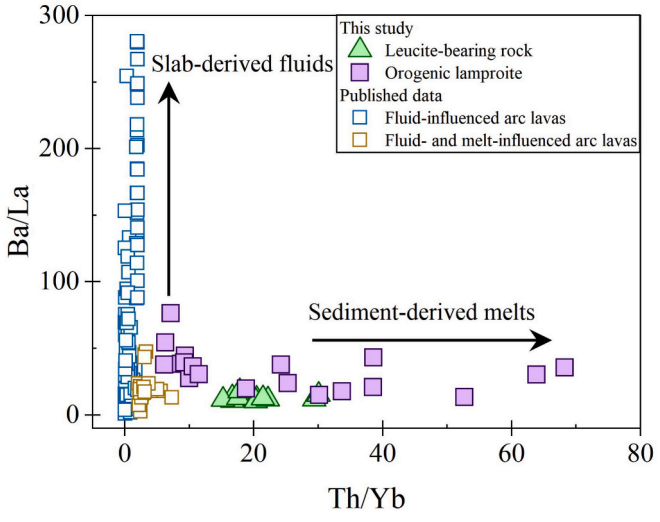

Fig. 8. Plots of Th/Yb ratios versus Ba/La ratios for the Mediterranean alkaline rocks investigated in this study and the compiled arc-related lavas from the Marianas and SW Pacific (Kendrick et al., 2020; Maunder et al., 2024). Th is enriched in sediment-derived melts as a fluid-immobile incompatible element, whereas Ba is preferentially enriched in slab-derived fluids as a fluid-mobile element.

display lower F/Cl (~0.58) and markedly higher F/Nd (~34.1) and Cl/Nb (~1315) than the sediment melt-dominated arc magmas (Figs. 9 and 10), indicating that slab-fluid metasomatism preferentially enriches Cl relative to F and produces pronounced fractionation of F/Nd and Cl/Nb in the mantle source (Kendrick et al., 2020; Maunder et al., 2024). Arc lavas inferred to have been influenced by both aqueous fluids and sediment melts show halogen characteristics similar to those of fluid-dominated arc lavas (Fig. 9), suggesting that the halogen signature of sediment melts is readily overprinted by aqueous slab fluids in these lavas (Maunder et al., 2024). Collectively, these results demonstrate that slab melting and dehydration exert fundamentally different controls on the halogen recycling in subduction zones, and that the combined F/Cl, F/Nd, and Cl/Nb systematics provide an effective means of distinguishing the respective contributions of slab melts and slab-derived fluids in arc magmatism.

5.6. Role of dehydrated subducted sediment in halogen recycling into the deep mantle

As indicated by the Mediterranean alkaline rocks studied here, melts derived from dehydrated subducted sediments can efficiently extract large amounts of F and Cl from the slab into the mantle wedge without producing significant fractionation of F/Nd or Cl/Nb. If dehydrated sediments can be transported into the deep mantle and undergo melting, they may likewise exert an important influence on halogen recycling in the deep mantle. To evaluate the potential contribution of dehydrated sediments to the sources of mantle-derived magmas, we compare the halogen data of the sediment-influenced Mediterranean alkaline rocks studied here with compiled data of E-MORB and OIB glasses and melt inclusions, as well as kimberlites (Supplementary Table 1).

We find that EM-type OIBs display relatively uniform F/Nd (~20.6) and Cl/Nb (~11.6), both of which largely overlap the range of primary N-MORB (Figs. 9 and 10). These values are also consistent with the halogen characteristics of our Mediterranean alkaline rocks interpreted to record dehydrated sediment-melt metasomatism (Figs. 9 and 10). The EM-type mantle sources are widely interpreted to involve recycled subducted sediments (Eisele et al., 2002; Jackson et al., 2007), this therefore suggests that melting of the dehydrated sediments in the deep mantle may contribute significantly to the halogen compositions of EM-type OIB sources. In contrast, E-MORB and HIMU-type OIB, which are commonly linked to recycled altered oceanic crust (e.g., Hanyu et al., 2019; Shimizu et al., 2016), show relatively uniform Cl/Nb (~19.4 and ~ 16.7, respectively; Figs. 9 and 10) that also overlap the N-MORB range, but distinctly elevated F/Nd (~30.4 and ~ 30.5, respectively; Figs. 9 and 10). Some HIMU even exhibit F/Nd values up to ~180 (Koleszar et al., 2009; Lassiter et al., 2002; Le Voyer et al., 2015). Such anomalously high F/Nd values may reflect the involvement of recycled altered igneous oceanic crust.

Kimberlites are deeply derived magmas generated by low-degree melting of mantle, however, available halogen data of these rocks remain scarce (Abersteiner et al., 2018; Hoare et al., 2021; Toyama et al., 2021). The compiled kimberlites exhibit Cl/Nb ratios lower than those of N-MORB (mean ≈ 1.9; Figs. 3 and 9), broadly overlapping the leucite-bearing rocks and most of the low-Cl/Nb lamproites investigated here (Figs. 3 and 9), suggesting variable degrees of Cl loss during degassing and that their Cl abundances may not reliably preserve primary-melt signatures. In contrast, the kimberlites exhibit a relatively restricted range of F/Nd ratios (11.1–26.0; mean = 16.5). Their mean F/Nd ratio is slightly lower than those of the Mediterranean alkaline rocks (~20.7) and EM-type OIB (~20.6), and substantially lower than those of E-MORB (~30.4) and HIMU-type OIB (~30.5; Fig. 9). These differences may indicate limited contributions from subducted dehydrated sediments and recycled AOC to the mantle sources of the compiled kimberlites. However, this interpretation remains tentative and requires further evaluation using multiple geochemical tracers. Overall, these results suggest that both recycled sediments and altered igneous oceanic

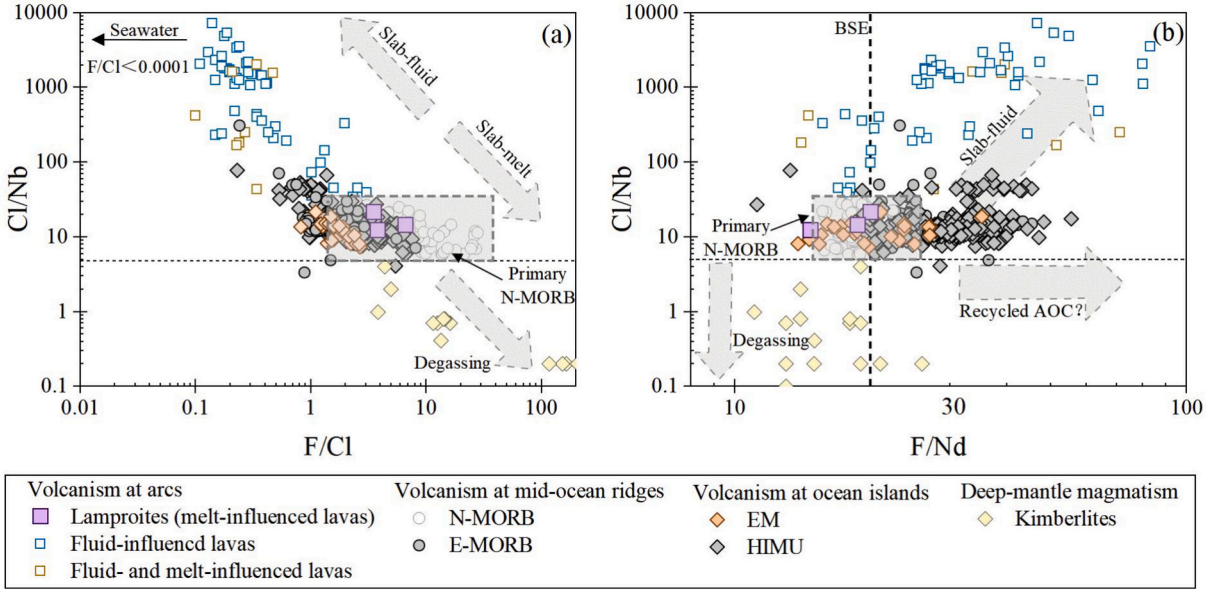

Fig. 9. Log-log plots of F/Cl versus Cl/Nb (a) and F/Nd versus Cl/Nb (b) for the Mediterranean alkaline rocks investigated in this study, together with compiled arc lavas, MORB, and OIB data. (a) Slab-fluid metasomatism and slab-melt metasomatism are characterized by decreases and increases in F/Cl, respectively; seawater data are from Kendrick et al. (2017); (b) Relative to primary N-MORB (grey box), the sediment-melt-influenced Mediterranean alkaline rocks and EM-type OIB show similar F/Nd and Cl/Nb ratios, whereas fluid-influenced and fluid- plus melt-influenced arc lavas are characterized by elevated Cl/Nb and F/Nd. In contrast, E-MORB and HIMU-type OIB display Cl/Nb ratios similar to those of N-MORB, but distinctly higher F/Nd.

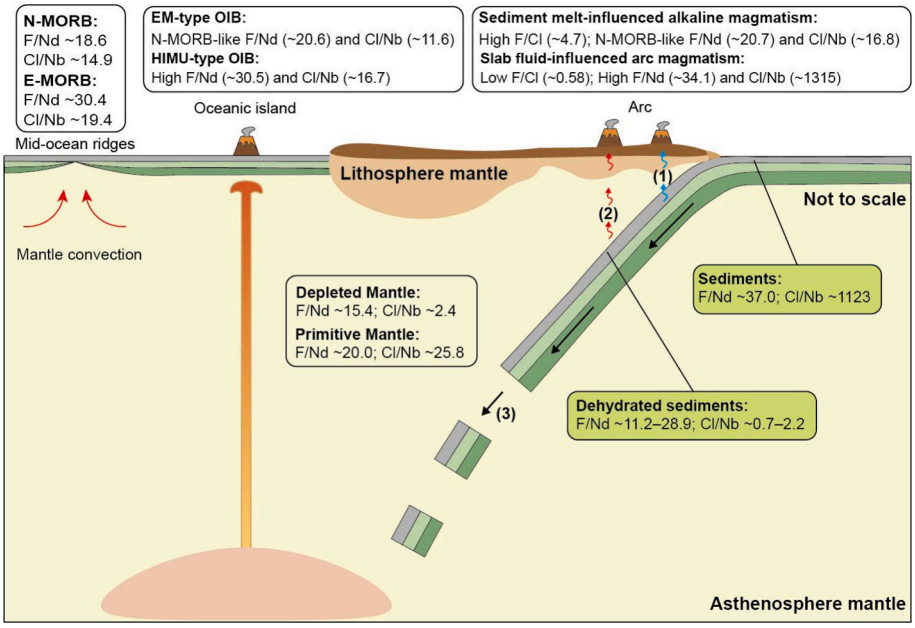

Fig. 10. An overview schematic of halogen recycling in the subduction zones and deep mantle, emphasizing variations in halogen ratios among major reservoirs and magmas. Geodynamic features are not to scale. During slab subduction, halogens are extracted from the slab through slab dehydration (1) and sediment melting (2), and are subsequently returned to the surface by arc magmatism. The remaining halogens are retained in the residual dehydrated slab, which may continue to subduct into the deep mantle (3) and further influence the halogen signatures of deep-sourced OIBs. Primitive mantle data are from McDonough and Sun (1995); Depleted mantle data are from Salters and Stracke (2004); Halogen data of sediment and dehydrated sediment are from Kendrick (2018) and Hughes et al. (2018), whereas Nb and Nd for sediment are from GLOSS (Plank and Langmuir, 1998). Data sources for MORB, OIB, and arc lavas are the same as those in Fig. 1.

crust can participate in halogen cycling in the deep mantle and make important contributions to the halogen compositions of OIB and E-MORB mantle sources.

6. Conclusions

We report whole-rock halogen (F and Cl), C, and S data, together with F/Cl, F/Nd, and Cl/Nb ratios, for Mediterranean alkaline rocks derived from mantle sources metasomatized by sediment melts. By further comparing these data with halogen systematics of arc magmas influenced by slab-derived fluids and OIBs linked to recycled slab components, this study provides new insights into the role of melting of dehydrated sediments in halogen cycling in subduction zones and the deep mantle. Our main conclusions are as follows:

1. After excluding significant modification by secondary alteration and magmatic processes, the F/Nd ratios of the leucite-bearing rocks and primitive lamproites (Mg# > 75) are inferred to approximate those of their mantle sources (13.5–24.6 and 14.8–26.9, respectively), whereas the Cl/Nb ratios of the least-degassed lamproites are inferred to approximate those of the lamproitic mantle source (12.2–21.5). These values are consistent with those of dehydrated subducted sediments. Combined with the high Th/Yb and low Ba/La ratios of these alkaline rocks, these results indicate that the halogen compositions of the mantle sources of the Mediterranean alkaline rocks were largely influenced by subducted dehydrated sediments.
2. Modeling calculations show that the mantle sources of the Mediterranean alkaline rocks studied here were substantially enriched in halogens relative to DMM, reaching levels comparable to ~50 × DMM (~800 ppm F and ~ 50 ppm Cl). This suggests that subducted dehydrated sediments can still transfer substantial halogen budgets into subduction zones and metasomatize the overlying mantle wedge through sediment melting, thereby generating the halogen-enriched mantle sources of the Mediterranean alkaline rocks studied here.
3. The combined systematics of F/Cl, F/Nd, and Cl/Nb provide an effective means of distinguishing the roles of sediment melting and slab dehydration in halogen recycling within subduction zones. Sediment-melt metasomatism enriches the mantle source in F and Cl without significantly fractionating F/Nd or Cl/Nb relative to depleted mantle. In contrast, slab-fluid metasomatism preferentially enriches Cl over F and produces pronounced fractionation of F/Nd and Cl/Nb in the mantle source.
4. The EM-type OIB, which are widely interpreted to involve recycled subducted sediments, display F/Nd and Cl/Nb ratios of ~20.6 and ~ 11.6, respectively, overlapping those of the Mediterranean alkaline rocks studied here. This correspondence suggests that dehydrated sediments also play an important role in the cycling of surface-derived halogens into the deep mantle and may contribute significantly to the halogen budget of EM-type OIB mantle sources.

CRediT authorship contribution statement

Qingxun Luo: Writing – original draft, Investigation, Formal analysis, Data curation. **Chunfei Chen:** Writing – review & editing, Writing – original draft, Supervision, Funding acquisition, Formal analysis, Data curation, Conceptualization. **Martina Casalini:** Writing – review & editing, Resources. **Dejan Prelević:** Writing – review & editing, Resources. **Sandro Conticelli:** Writing – review & editing, Resources. **Michael W. Förster:** Writing – review & editing. **Stephen F. Foley:** Writing – review & editing, Funding acquisition. **Xu Xiao:** Writing – review & editing, Investigation. **Tao He:** Resources, Methodology. **Zhaochu Hu:** Resources, Methodology. **Yongsheng Liu:** Resources, Methodology.

Acknowledgements

CC is deeply grateful to Professor Stephen F. Foley for his generous mentorship and support during the early stages of CC's research career. This research is funded by the Key R&D Program of China (2024YFF0808200), the National Natural Science Foundation of China (42573048 and 42573027), and the Hubei Provincial Natural Science Foundation of China (Grant No. 2026AFA122). SF is supported by MOST Special Fund from SKL-GPMR (GPMR202501) and ARC grant FL180100134. We thank Guest Editor Sebastian Tappe, reviewer Stephan Klemme, and an anonymous reviewer for their constructive comments and suggestions, which greatly improved the manuscript.

Appendix A. Supplementary data

Supplementary data to this article can be found online at https://doi.org/10.1016/j.lithos.2026.108777.

References

Abersteiner, A., et al., 2018. Significance of halogens (F, Cl) in kimberlite melts: Insights from mineralogy and melt inclusions in the Roger pipe (Ekati, Canada). Chem Geol 478, 148–163.
Ammannati, E., Jacob, D.E., Avanzinelli, R., Foley, S.F., Conticelli, S., 2016. Low Ni olivine in silica-undersaturated ultrapotassic igneous rocks as evidence for carbonate metasomatism in the mantle. Earth Planet Sci Lett 444, 64–74.
Avanzinelli, R., Elliott, T., Tommasini, S., Conticelli, S., 2008. Constraints on the genesis of potassium-rich Italian volcanic rocks from U/Th disequilibrium. J Petrol 49 (2), 195–223.
Avanzinelli, R., Lustrino, M., Mattei, M., Melluso, L., Conticelli, S., 2009. Potassic and ultrapotassic magmatism in the circum-Tyrrhenian region: significance of carbonated pelitic vs. pelitic sediment recycling at destructive plate margins. Lithos 113 (1), 213–227.
Balcone-Boissard, H., Michel, A., Villemant, B., 2009. Simultaneous determination of fluorine, chlorine, bromine and iodine in six geochemical reference materials using pyrohydrolysis, ion chromatography and inductively coupled plasma-mass spectrometry. Geostand Geoanal Res 33 (4), 477–485.
Behn, M.D., Kelemen, P.B., Hirth, G., Hacker, B.R., Massonne, H.-J., 2011. Diapirs as the source of the sediment signature in arc lavas. Nat Geosci 4 (9), 641–646.
Boari, E., et al., 2009. Isotope geochemistry (Sr–Nd–Pb) and petrogenesis of leucite-bearing volcanic rocks from "Colli Albani" volcano, Roman Magmatic Province, Central Italy: inferences on volcano evolution and magma genesis. Bull Volcanol 71 (9), 977–1005.
Cabral, R.A., et al., 2014. Volatile cycling of H2O, CO2, F, and Cl in the HIMU mantle: a new window provided by melt inclusions from oceanic hot spot lavas at Mangaia, Cook Islands. Geochem Geophys Geosyst 15 (11), 4445–4467.
Cadoux, A., et al., 2018. The role of melt composition on aqueous fluid vs. silicate melt partitioning of bromine in magmas. Earth Planet Sci Lett 498, 450–463.
Casalini, M., et al., 2022. Petrogenesis of Mediterranean lamproites and associated rocks: The role of overprinted metasomatic events in the post-collisional lithospheric upper mantle. Geol Soc Lond Spec Publ 513 (1), 271–296.
Cavazza, W., Wezel, F., 2003. The Mediterranean region- a geological primer. Episodes 26 (3), 160–168.
Cavazza, W., Roure, F., Ziegler, P.A., 2004. The Mediterranean Area and the Surrounding Regions: Active Processes, Remnants of Former Tethyan Oceans and Related Thrust Belts. In: Cavazza, W., Roure, F., Spakman, W., Stampfli, G.M., Ziegler, P.A. (Eds.), The TRANSMED Atlas. The Mediterranean Region from Crust to Mantle: Geological and Geophysical Framework of the Mediterranean and the Surrounding Areas. Springer Berlin Heidelberg, Berlin, Heidelberg, pp. 1–29.
Chen, C., 2025. Halogen composition and heterogeneity in the continental lithospheric mantle. Sci China Earth Sci 68 (1), 310–314.
Chen, C., Förster, M.W., Foley, S.F., Liu, Y., 2021. Massive carbon storage in convergent margins initiated by subduction of limestone. Nat Commun 12 (1), 4463.
Chen, C., Forster, M.W., Foley, S.F., Shcheka, S.S., 2023. Carbonate-rich crust subduction drives the deep carbon and chlorine cycles. Nature 620 (7974), 576–581.
Condamine, P., Médard, E., 2014. Experimental melting of phlogopite-bearing mantle at 1 GPa: implications for potassic magmatism. Earth Planet Sci Lett 397, 80–92.
Conticelli, S., Avanzinelli, R., Ammannati, E., Casalini, M., 2015. The role of carbon from recycled sediments in the origin of ultrapotassic igneous rocks in the Central Mediterranean. Lithos 232, 174–196.
Dalou, C., Koga, K.T., Shimizu, N., Boulon, J., Devidal, J.-L., 2012. Experimental determination of F and Cl partitioning between lherzolite and basaltic melt. Contrib Mineral Petrol 163 (4), 591–609.
Dalou, C., Koga, K.T., Le Voyer, M., Shimizu, N., 2014. Contrasting partition behavior of F and Cl during hydrous mantle melting: implications for Cl/F signature in arc magmas. Prog Earth Planet Sci 1 (1), 26.
Defant, M.J., Drummond, M.S., 1990. Derivation of some modern arc magmas by melting of young subducted lithosphere. Nature 347 (6294), 662–665.
Eisele, J., et al., 2002. The role of sediment recycling in EM-1 inferred from Os, Pb, Hf, Nd, Sr isotope and trace element systematics of the Pitcairn hotspot. Earth Planet Sci Lett 196 (3), 197–212.
El-Sharkawy, A., et al., 2020. The slab puzzle of the Alpine-Mediterranean region: insights from a new, high-resolution, shear wave velocity model of the upper mantle. Geochem Geophys Geosyst 21 (8), e2020GC008993.
Erman, C., et al., 2022. Constraints on the lithospheric kinematics in the Aegean and Western Anatolia unveiled by SKS splitting observations. J Geophys Res Solid Earth 127 (12), e2022JB025265.
Faccenna, C., Becker, T.W., Lucente, F.P., Jolivet, L., Rossetti, F., 2001. History of subduction and back arc extension in the Central Mediterranean. Geophys J Int 145 (3), 809–820.
Flemetakis, S., et al., 2021. Constraining the presence of amphibole and mica in metasomatized mantle sources through halogen partitioning experiments. Lithos 380-381, 105859.
Foley, S.F., 1989. Experimental constraints of phlogopite chemistry in lamproites; 1, The effect of water activity and oxygen fugacity. Eur J Mineral 1 (3), 411–426.
Foley, S.F., Ezad, I.S., 2024. Melting of hydrous pyroxenites with alkali amphiboles in the continental mantle: 2. Trace element compositions of melts and minerals. Geosci Front 15 (1), 101692.
Frezzotti, M.L., Ferrando, S., 2018. The Role of Halogens in the Lithospheric Mantle. In: Harlov, D.E., Aranovich, L. (Eds.), The Role of Halogens in Terrestrial and Extraterrestrial Geochemical Processes: Surface, Crust, and Mantle. Springer International Publishing, Cham, pp. 805–845.
Gerya, T.V., Yuen, D.A., 2003. Rayleigh–Taylor instabilities from hydration and melting propel 'cold plumes' at subduction zones. Earth Planet Sci Lett 212 (1), 47–62.

Grégoire, M., Moine, B.N., O'Reilly, S.Y., Cottin, J.Y., Giret, A., 2000. Trace element residence and partitioning in mantle xenoliths metasomatized by highly alkaline, silicate- and carbonate-rich melts (Kerguelen Islands, Indian Ocean). J Petrol 41 (4), 477–509.
Gutscher, M.-A., Maury, R., Eissen, J.-P., Bourdon, E., 2000. Can slab melting be caused by flat subduction? Geology 28 (6), 535–538.
Han, P., et al., 2023. Halogen (F, Cl, Br, and I) concentrations of the upper continental crust through time as recorded in ancient glacial diamictite composites. Geochim Cosmochim Acta 341, 28–45.
Hanano, D., Weis, D., Scoates, J.S., Aciego, S., DePaolo, D.J., 2010. Horizontal and vertical zoning of heterogeneities in the Hawaiian mantle plume from the geochemistry of consecutive postshield volcano pairs: Kohala-Mahukona and Mauna Kea–Hualalai. Geochem Geophys Geosyst 11 (1).
Hanyu, T., et al., 2019. Tiny droplets of ocean island basalts unveil Earth's deep chlorine cycle. Nat Commun 10 (1), 60.
He, T., et al., 2019. Determination of Cl, Br, and I in geological materials by sector field inductively coupled plasma mass spectrometry. Anal Chem 91 (13), 8109–8114.
Hoare, B.C., et al., 2021. Tracking halogen recycling and volatile loss in kimberlite magmatism from Greenland: evidence from combined F-Cl-Br and δ37Cl systematics. Lithos 384–385.
Hughes, L., et al., 2018. Halogen behaviour in subduction zones: eclogite facies rocks from the Western and Central Alps. Geochim Cosmochim Acta 243, 1–23.
Jackson, M.G., et al., 2007. The return of subducted continental crust in Samoan lavas. Nature 448 (7154), 684–687.
Jackson, M.G., et al., 2015. Deeply dredged submarine HIMU glasses from the Tuvalu Islands, Polynesia: implications for volatile budgets of recycled oceanic crust. Geochem Geophys Geosyst 16 (9), 3210–3234.
John, T., Scambelluri, M., Frische, M., Barnes, J.D., Bach, W., 2011. Dehydration of subducting serpentinite: implications for halogen mobility in subduction zones and the deep halogen cycle. Earth Planet Sci Lett 308 (1), 65–76.
Kendrick, M.A., 2018. Halogens in Seawater, Marine Sediments and the Altered Oceanic Lithosphere. In: Harlov, D.E., Aranovich, L. (Eds.), The Role of Halogens in Terrestrial and Extraterrestrial Geochemical Processes: Surface, Crust, and Mantle. Springer International Publishing, Cham, pp. 591–648.
Kendrick, M.A., 2024. Halogen cycling in the solid earth. Annu Rev Earth Planet Sci 52 (1), 195–220.
Kendrick, M.A., et al., 2014. Subduction-related halogens (Cl, Br and I) and H2O in magmatic glasses from Southwest Pacific Backarc Basins. Earth Planet Sci Lett 400, 165–176.
Kendrick, M.A., et al., 2017. Seawater cycled throughout Earth's mantle in partially serpentinized lithosphere. Nat Geosci 10 (3), 222–228.
Kendrick, M.A., et al., 2020. SW Pacific arc and backarc lavas and the role of slab-bend serpentinites in the global halogen cycle. Earth Planet Sci Lett 530.
Kirstein, L.A., et al., 2023. Volatiles and intraplate magmatism: a variable role for carbonated and altered Oceanic lithosphere in Ocean Island Basalt formation. J Petrol 64 (5).
Kjarsgaard, B.A., Pearson, D.G., Tappe, S., Nowell, G.M., Dowall, D.P., 2009. Geochemistry of hypabyssal kimberlites from Lac de Gras, Canada: comparisons to a global database and applications to the parent magma problem. Lithos 112, 236–248.
Klemme, S., Blundy, J.D., Wood, B.J., 2002. Experimental constraints on major and trace element partitioning during partial melting of eclogite. Geochim Cosmochim Acta 66 (17), 3109–3123.
Kobayashi, M., Sumino, H., Saito, T., Nagao, K., 2021. Determination of halogens in geological reference materials using neutron irradiation noble gas mass spectrometry. Chem Geol 582, 120420.
Koleszar, A.M., et al., 2009. The volatile contents of the Galapagos plume; evidence for H_2O and F open system behavior in melt inclusions. Earth Planet Sci Lett 287 (3), 442–452.
Lassiter, J.C., Hauri, E.H., Nikogosian, I.K., Barsczus, H.G., 2002. Chlorine–potassium variations in melt inclusions from Raivavae and Rapa, Austral Islands: constraints on chlorine recycling in the mantle and evidence for brine-induced melting of oceanic crust. Earth Planet Sci Lett 202 (3), 525–540.
Le Voyer, M., Cottrell, E., Kelley, K.A., Brounce, M., Hauri, E.H., 2015. The effect of primary versus secondary processes on the volatile content of MORB glasses: An example from the equatorial Mid-Atlantic Ridge (5°N–3°S). J Geophys Res Solid Earth 120 (1), 125–144.
Lesne, P., et al., 2011. Experimental simulation of closed-system degassing in the system basalt–H2O–CO2–S–Cl. J Petrol 52 (9), 1737–1762.
Li, H., Hermann, J., Zhang, L., 2022. Melting of subducted slab dictates trace element recycling in global arcs. Sci Adv 8 (2), eabh2166.
Mann, U., Schmidt, M.W., 2015. Melting of pelitic sediments at subarc depths: 1. Flux vs. fluid-absent melting and a parameterization of melt productivity. Chem Geol 404, 150–167.
Marschall, H.R., Schumacher, J.C., 2012. Arc magmas sourced from mélange diapirs in subduction zones. Nat Geosci 5 (12), 862–867.
Maunder, B.L., Kendrick, M.A., Ribeiro, J.M., Nebel, O., 2024. A negligible role for forearc serpentinites and mélange diapirism in contributing halogens to Mariana arc magmas. Earth Planet Sci Lett 625, 118498.
McDonough, W.F., Sun, S.s., 1995. The composition of the Earth. Chem Geol 120 (3), 223–253.
Muramatsu, Y., Fehn, U., Yoshida, S., 2001. Recycling of iodine in fore-arc areas: evidence from the iodine brines in Chiba, Japan. Earth Planet Sci Lett 192 (4), 583–593.
Muramatsu, Y., et al., 2007. Halogen concentrations in pore waters and sediments of the Nankai Trough, Japan: implications for the origin of gas hydrates. Appl Geochem 22 (3), 534–556.
Néron, A., Bédard, L.P., Gaboury, D., 2018. The Saint-Honoré Carbonatite REE zone, Québec, Canada: combined magmatic and hydrothermal processes. Minerals 8 (9), 397.
Niu, Y., 1997. Mantle melting and melt extraction processes beneath ocean ridges: evidence from Abyssal peridotites. J Petrol 38 (8), 1047–1074.
O'Reilly, S.Y., Griffin, W.L., 2000. Apatite in the mantle: implications for metasomatic processes and high heat production in Phanerozoic mantle. Lithos 53 (3), 217–232.
Pagé, L., Hattori, K., 2019. Abyssal serpentinites: transporting halogens from Earth's surface to the deep mantle. Minerals 9 (1), 61.
Peccerillo, A., Frezzotti, M.L., 2015. Magmatism, mantle evolution and geodynamics at the converging plate margins of Italy. J Geol Soc Lond 172 (4), 407–427.
Plank, T., Langmuir, C.H., 1998. The chemical composition of subducting sediment and its consequences for the crust and mantle. Chem Geol 145 (3), 325–394.
Prelević, D., Foley, S.F., Romer, R.L., Cvetković, V., Downes, H., 2005. Tertiary ultrapotassic volcanism in Serbia: constraints on petrogenesis and mantle source characteristics. J Petrol 46 (7), 1443–1487.
Prelević, D., Foley, S.F., Cvetković, V., 2007. A review of petrogenesis of Mediterranean Tertiary lamproites: a perspective from the Serbian ultrapotassic province. In: Beccaluva, L., Bianchini, G., Wilson, M. (Eds.), Cenozoic Volcanism in the Mediterranean Area. Geological Society of America, pp. 113–129.
Prelević, D., Foley, S.F., Romer, R., Conticelli, S., 2008. Mediterranean Tertiary lamproites derived from multiple source components in postcollisional geodynamics. Geochim Cosmochim Acta 72 (8), 2125–2156.
Prelević, D., et al., 2012. Ultrapotassic mafic rocks as geochemical proxies for post-collisional dynamics of orogenic lithospheric mantle: the case of Southwestern Anatolia, Turkey. J Petrol 53 (5), 1019–1055.
Ren, H., et al., 2024. Calcium isotope compositions of subduction-related leucite-bearing rocks: implications for the calcium isotope heterogeneity of the mantle and carbonate recycling in convergent margins. Geochim Cosmochim Acta 364, 100–113.
Robertson, A., Karamata, S., Šarić, K., 2009. Overview of ophiolites and related units in the Late Palaeozoic–Early Cenozoic magmatic and tectonic development of Tethys in the northern part of the Balkan region. Lithos 108 (1), 1–36.
Salters, V.J.M., Stracke, A., 2004. Composition of the depleted mantle. Geochem Geophys Geosyst 5 (5).
Schmid, S.M., et al., 2020. Tectonic units of the Alpine collision zone between Eastern Alps and western Turkey. Gondwana Res 78, 308–374.
Schmidt, K.H., Bottazzi, P., Vannucci, R., Mengel, K., 1999. Trace element partitioning between phlogopite, clinopyroxene and leucite lamproite melt. Earth Planet Sci Lett 168 (3), 287–299.
Sekimoto, S., Ebihara, M., 2017. Accurate determination of chlorine, bromine and iodine in U.S. Geological survey geochemical reference materials by radiochemical neutron activation analysis. Geostand Geoanal Res 41 (2), 213–219.
Sha, L.-K., Chappell, B.W., 1999. Apatite chemical composition, determined by electron microprobe and laser-ablation inductively coupled plasma mass spectrometry, as a probe into granite petrogenesis. Geochim Cosmochim Acta 63 (22), 3861–3881.
Shimizu, K., et al., 2016. Two-component mantle melting-mixing model for the generation of mid-ocean ridge basalts: Implications for the volatile content of the Pacific upper mantle. Geochim Cosmochim Acta 176, 44–80.
Sides, I., et al., 2014. Magma mixing and high fountaining during the 1959 Kīlauea Iki eruption, Hawai'i. Earth Planet Sci Lett 400, 102–112.
Sisson, T.W., Kimura, J.I., Coombs, M.L., 2009. Basanite–nephelinite suite from early Kilauea: carbonated melts of phlogopite–garnet peridotite at Hawaii's leading magmatic edge. Contrib Mineral Petrol 158 (6), 803–829.
Slovenec, D., Pamić, J., 2002. Geology of the Vardar zone ophiolites of the Medvednica mountain area located along the Zagreb-Zemplin line (NW Croatia). Geol Carpath 53, 53–59.
Straub, S.M., Layne, G.D., 2003. The systematics of chlorine, fluorine, and water in Izu arc front volcanic rocks: Implications for volatile recycling in subduction zones. Geochim Cosmochim Acta 67 (21), 4179–4203.
Tappe, S., Graham Pearson, D., Kjarsgaard, B.A., Nowell, G., Dowall, D., 2013. Mantle transition zone input to kimberlite magmatism near a subduction zone: origin of anomalous Nd–Hf isotope systematics at Lac de Gras, Canada. Earth Planet Sci Lett 371-372, 235–251.
Teiber, H., et al., 2014. The distribution of halogens (F, Cl, Br) in granitoid rocks. Chem Geol 374-375, 92–109.
Toyama, C., et al., 2021. Halogen heterogeneity in the subcontinental lithospheric mantle revealed by I/Br ratios in kimberlites and their mantle xenoliths from South Africa, Greenland, China, Siberia, Canada, and Brazil. Am Mineral 106 (12), 1890–1899.
Ustaszewski, K., et al., 2010. Evolution of the Adria-Europe plate boundary in the northern Dinarides: from continent-continent collision to back-arc extension. Tectonics 29 (6).
Villemant, B., Mouatt, J., Michel, A., 2008. Andesitic magma degassing investigated through H2O vapour–melt partitioning of halogens at Soufrière Hills Volcano, Montserrat (Lesser Antilles). Earth Planet Sci Lett 269 (1), 212–229.
Wang, L., et al., 2025. Chalcophile element contents of coeval volcanic rocks derived from heterogeneous mantle beneath North China Craton. Lithos 516-517, 108273.
Wang, Q., Makishima, A., Nakamura, E., 2010. Determination of fluorine and chlorine by pyrohydrolysis and ion chromatography: comparison with alkaline fusion digestion and ion chromatography. Geostand Geoanal Res 34 (2), 175–183.

Wang, Y., Xu, Y.-G., 2024. Volatiles in the mantle transition zone and their effects on big mantle wedge systems. Natl Sci Rev 11 (6), nwae136.
Webster, J.D., Baker, D.R., Aiuppa, A., 2018. Halogens in Mafic and Intermediate-Silica Content Magmas. In: Harlov, D.E., Aranovich, L. (Eds.), The Role of Halogens in Terrestrial and Extraterrestrial Geochemical Processes: Surface, Crust, and Mantle. Springer International Publishing, Cham, pp. 307–430.
Zheng, Y., et al., 2023. Heavy halogen compositions of lamprophyres derived from metasomatized lithospheric mantle beneath eastern North China Craton. Am Mineral 108 (10), 1825–1839.